Crystallization control of $CaO-SiO_2-Al_2O_3-MgO$ system inclusion

Yong Wang[1,2,3], Sohei Sukenaga[2], Wangzhong Mu[3], Hua Zhang[1], Hongwei Ni[1], Hiroyuki Shibata[2]

1. The State Key Laboratory of Refractories and Metallurgy, Wuhan University of Science and Technology, Wuhan, 430081, China
2. Institute of Multidisciplinary Research for Advanced Materials, Tohoku University, 2-1-1 Katahira, Aoba-ku, Sendai, Miyagi 980-8577, Japan
3. Department of Materials Science and Engineering, KTH Royal Institute of Technology, Stockholm, 10044, Sweden

Keywords: crystallization, non-metallic inclusions, thermodynamic and kinetic, Si-Mn deoxidation

ABSTRACT

The crystallization behavior of low melting point $CaO-SiO_2-Al_2O_3-MgO$ inclusions greatly affect the deformability of inclusions during the rolling process. The crystallization characteristics of $CaO-SiO_2-Al_2O_3-MgO$ melts representing the oxide inclusions in Si-Mn killed steel were systematically investigated. The effect of Al_2O_3 and MgO contents on the crystallization change was analyzed under a fixed CaO/ SiO_2 in the complex inclusions. The continuous-cooling-transformation (CCT) and time-temperature-transformation (TTT) experiments were conducted. The results showed that the increase of MgO content increases the crystallization ability of $CaO-SiO_2-Al_2O_3-MgO$ inclusions, while the increase of Al_2O_3 content has the opposite effect. The viscosity, liquidus temperature of oxide melt and also the initial crystallization potential might be the reasons for the change in crystallization behavior. Also, the crystallization activation energy could semi-quantitatively characterize the crystal growth during the crystallization of inclusions. To obtain low melting point plasticized $CaO-SiO_2-Al_2O_3-MgO$ ($CaO/ SiO_2=1$) system inclusions, the Al_2O_3 content of the system needs to be controlled larger than 15 wt.% and the MgO content should be kept at a small amount.

1. INTRODUCTION

Inclusion control is one of the key areas in the clean steel production research since it directly affect the quality of final steel products. Till now, the inclusion evolution during refining and solidification processes has been widely studied in various steel grades.[1] Therefore, there is quite enough information on the inclusion control in the molten and solidification state of steel. However, the inclusion characteristics in the final products are usually not the same as them in the as cast steel. This is due to the fact that inclusions can also evolve changes in the heating and rolling process because the combined effect of thermal and mechanical treatments. Kitamura[2] pointed out the new directions of inclusion control should be focused on the heating, rolling deformation and cooling processes instead of refining and casting processes. Recent years, the inclusion characteristics during heat treatment as well as hot and cold rolling process have been investigated.[3, 4] The deformation ability of inclusions has a direct impact on the fatigue resistance of steel. Controlling the deformation performance of inclusions is one of the keys to improving the quality of high-end special steel. In order to improve the deformability of inclusions, the high melting point and non-deformable inclusions (such as Al_2O_3, $MgO-Al_2O_3$ spinel) should be removed as much as possible in steel. This is especially important in some specific steel types, such as spring steel and tire cord steel. Therefore, Si-Mn deoxidation is used instead of Al deoxidation in these steels. $CaO-SiO_2-Al_2O_3-MgO$ system oxide is a typical inclusion type in Si-Mn deoxidized steel. A larger number of studies aimed to control these inclusions in low melting point region to obtain better deformability. However, low melting point inclusions with high crystallization ability tend to crystalize during the soaking process before hot rolling, which can greatly decrease the deformation ability of inclusions during the rolling process. The crystallization behavior of oxide melts is commonly studied in glass ceramics, mold fluxes, and molten slags. However, there are few studies concerning the crystallization of oxide non-metallic inclusions in steel.

In this study, the effects of MgO and Al_2O_3 contents on the crystallization behavior of $CaO-SiO_2-Al_2O_3-MgO$ system inclusions were investigated using the sessile drop technique and thermodynamic calculations. This study provides a theoretical basis for understanding the crystallization behavior of $CaO-SiO_2-Al_2O_3-MgO$ system inclusions and optimization of its compositions with the lowest crystallization ability.

2. EXPERIMENTAL METHODS

2.1 Sample preparation

The compositions of oxide melt were firstly designed based on the typical compositions of the inclusions in Si-Mn killed steel, the range of composition is presented in Table 1. In total, there are 7 groups of sample, where the basicity (CaO/SiO_2) keeps as 1. In groups S1, S2, S3, S4, the MgO content fixes as 8%, and Al_2O_3 content varies from 5% to 20%. While in groups S2, S5, S6, S7, the Al2O3 content fixes as 10%, and MgO content varies from 4% to 16%. The oxide samples were prepared using reagent-grade powders of $CaCO_3$ (≥99.0 mass%), Al_2O_3 (≥99.99 mass %), MgO (≥98.50 mass%), SiO_2 (≥99.99 mass%). About 20 g oxide mixtures were placed in a platinum

crucible and melted in $MoSi_2$ furnace at 1600 ℃ for 1 hour to ensure the homogenization of chemical composition. Thereafter, the molten melt was quickly quenched on copper plate to obtain glass samples. The chemical compositions of the quenched samples were analyzed using X-Ray fluoroscopy (XRF) and listed in Table 1.

The crystallization behavior of the oxide melt was determined using a sessile drop measurement apparatus, which widely used for the wettability measurements[14, 15] as well as crystallization control.[16] The gas-tight furnace with customized apparatus is shown in Figure 2, which can allow us to observe the morphology change of melt and crystallization behavior in both vertical and horizontal directions. The whole heating and cooling process of samples were recorded by a CCD camera at the top, which was connected to a computer. About 50 mg glass sample was placed on a platinum substrate, which in turn, was placed on a platinum plate (diameter 13.0 mm; thickness 1.4 mm) on an Al_2O_3 tube pedestal. A sapphire plate was placed between the two-platinum holder. The temperature was measured using a thermocouple that was welded to the back of the platinum plate. Before the start of the experiment, the chamber was cleaned thoroughly by a cycle of vacuum and purging with a high purity Ar (purity>99.9999%). Then, the samples were heated up through quartz plates by two halogen lamps under an Ar protected atmosphere. The temperature profile for CCT and TTT experiments are shown in Figure 2. For both CCT and TTT experiments, the sample was heated to 1500 ℃ and kept for 3 minutes to eliminate the bubbles and uniform the chemical composition. Thereafter, the molten samples were continuously cooled at different cooling rates ranging from 5 ℃/min to 900 ℃/min in the CCT tests. In TTT experiments, the molten melt was cooling down rapidly to different temperatures ranging from 950 ℃ to 1250 ℃ at a cooling rate of 900 ℃/min. The iso-thermal treatment time for TTT tests are about 2 hours. In TTT experiments, the temperature and time at which 5 vol pct. of melt crystallized was determined as the start crystallization temperature and time, respectively.

TABLE 1 – Chemical compositions of oxide mixtures before and after pre-melting (mass%).

Sample No.	**Designed composition**			
	CaO	SiO_2	Al_2O_3	MgO
S1	43.5	43.5	5	8
S2	41	41	10	8
S3	38.5	38.5	15	8
S4	36	36	20	8
S5	43	43	10	4
S6	39	39	10	12
S7	37	37	10	16

2.2 Characterization methods

The crystallization characteristics of each sample were measured by ImageJ software, according to the difference of brightness and contrast between the crystals and the melt. In this study, the structures of the quenched oxide melt were analyzed using a laser confocal Raman spectrometer in order to reveal the relationship between the composition change and structure. The Raman spectra of the samples were recorded in the range of 200 $^{-1}$ to 2000 cm^{-1} at room temperature with the light source of a 1-mW semiconductor and an excitation wavelength of 500 nm. The solidified samples after the isothermal heat treatment experiments were divided into two parts, one part was crushed and grounded for XRD analysis in order to obtain the information of crystalline phases. The XRD data were collected using Cu Kα radiation in a range of 2θ=10-90 degree. The other part was cold mounted in epoxy resin, and grinded, polished, then the crystallized phases were determined by a field-emission scanning electron microscope (FESEM) equipped with energy dispersive X-ray spectroscopy (EDS; Bruker).

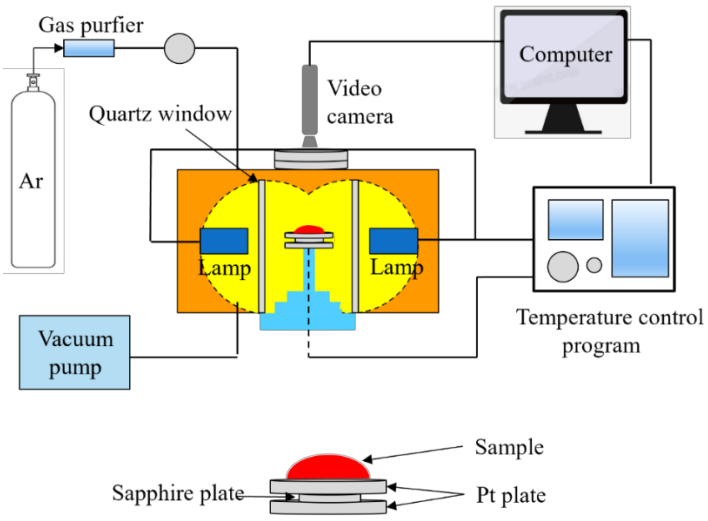

FIG 1 – Schematic diagram of the apparatus used to observe crystallization behavior.

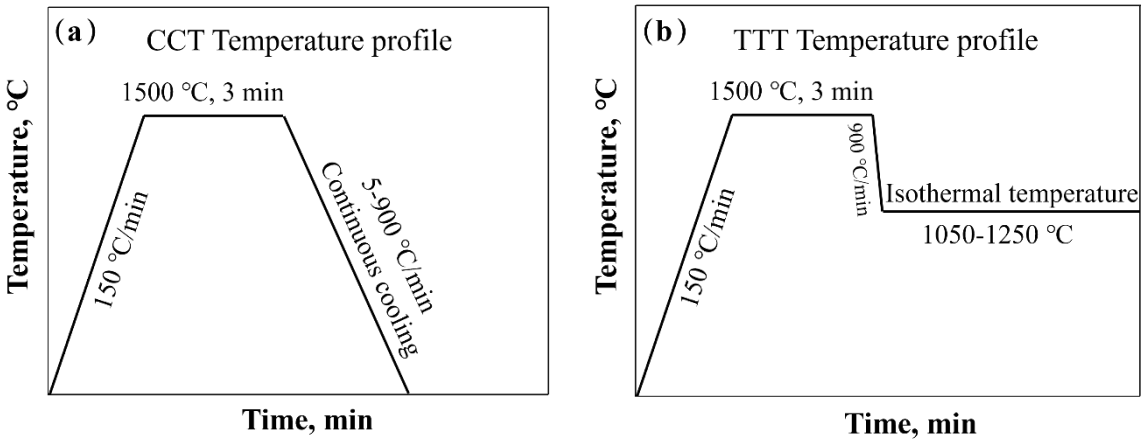

FIG 2 –Temperature profile of (a) CCT and (b) TTT tests.

3. RESULTS AND DISCUSSION

3.1 Continuous cooling crystallization behavior

During the continuous cooling experiment, the crystallization happens under a certain supercooling degree. Besides, the supercooling degree varies with the cooling rates and chemical compositions. Figure 3 shows the morphology of the crystals in the samples with varying MgO contents and cooling rates after the CCT experiment. It can be clearly seen that crystallization easily happens at a lower cooling rate and the crystallization tendency decreases with the cooling rate. When the MgO content is 4 %, fully crystallization can be seen for the sample at a cooling rate of 7.5. Two bulk crystals can be found for the sample at a cooling rate of 25, and the samples is transparent with no crystals at a cooling rate of 45. A higher cooling rate results in a higher supercooling degree, which decreases the driving force for the crystallization. Moreover, the crystallization tendency greatly increases with the increase of MgO contents. This is due to the fact that the fully crystallization happens under a cooling rate of 7.5 with 4% MgO content, and it happens under a cooling rate of 240 with 16% MgO content. In terms of Al_2O_3 effect, the crystallization tendency greatly decreases with the increase of Al_2O_3 contents.

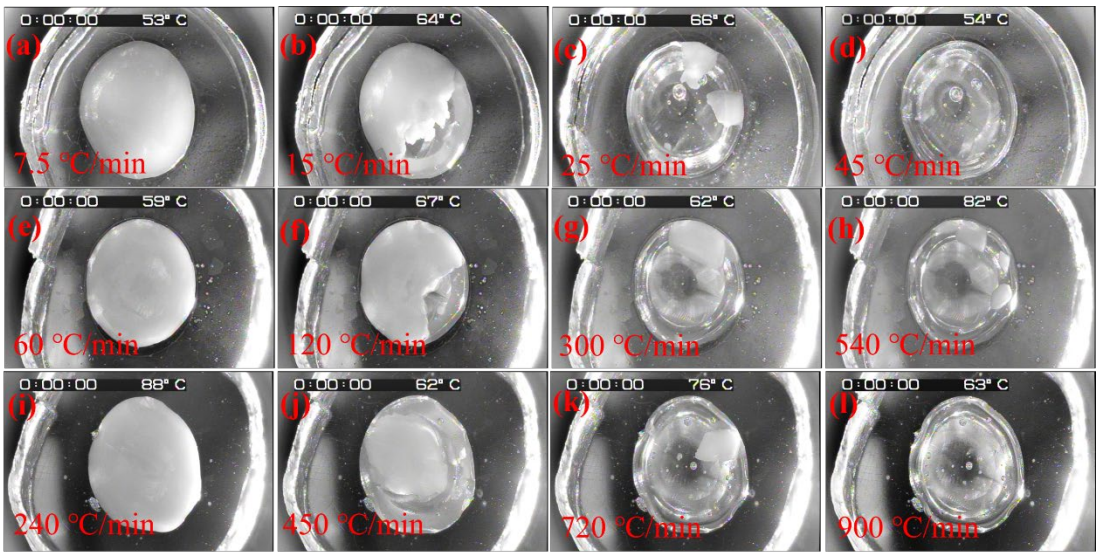

FIG 3– The morphology of crystals after the CCT experiments with varying MgO contents.

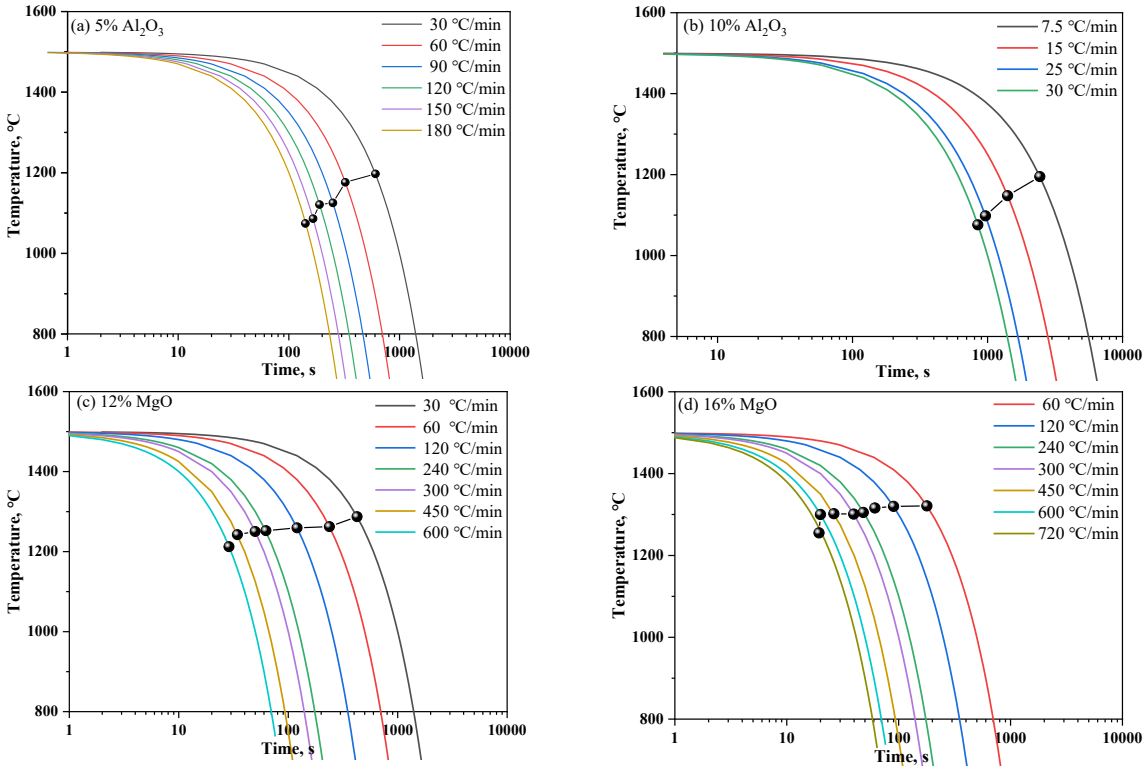

FIG 4 –CCT diagrams of CaO-SiO_2-Al_2O_3-MgO system inclusions with different compositions of (a) 5% Al_2O_3, (b) 10% Al_2O_3, (c) 12% MgO, and (d) 16% MgO.

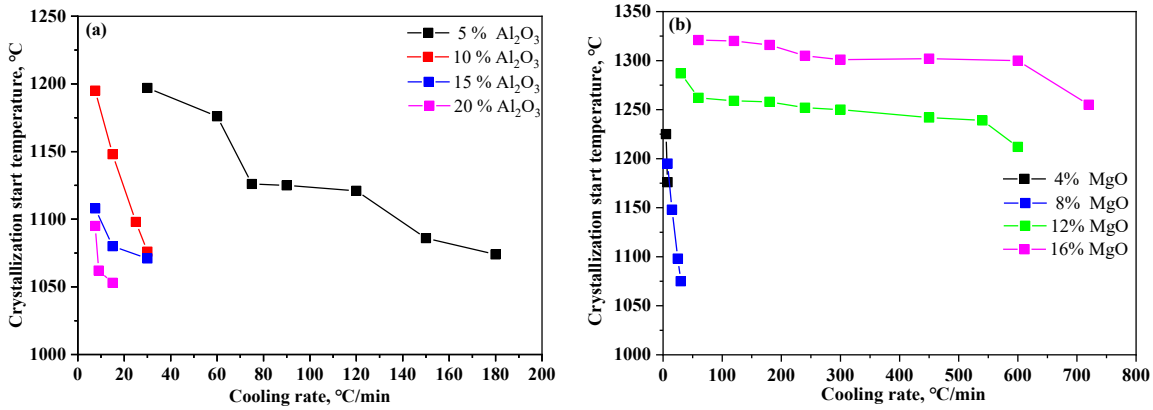

FIG 5 –The start crystallization temperature in sample with varied (a) Al_2O_3 and (b) MgO contents.

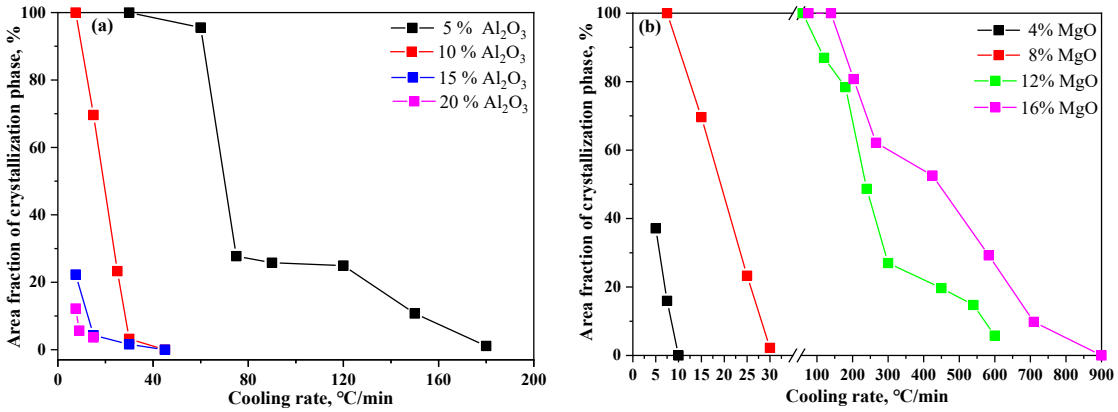

FIG 6 –The area fractions of crystallization phases in sample with varied (a) Al_2O_3 and (b) MgO contents.

Systematic analysis of the crystallization characteristics based on the CCT experiments were performed. Figure 4 presents the CCT diagrams of the samples with varying Al_2O_3 and MgO contents. There are three obvious areas, a liquid area in a higher temperature, a crystallization area in the middle and a glass area in a lower temperature. The critical cooling rate and the start crystallization temperature are important parameters for evaluating the crystallization ability of the samples. Taken the sample with 5% Al_2O_3 as an example (Figure 4 (a)), crystals can be formed when the cooling rate smaller than 180 ℃/min, and the sample will be glass when the cooling rate larger than 180 ℃/min. Thus, the critical cooling rate can be determined to be 180 ℃/min. It should be noticed that the critical cooling rate greatly increases from 30 ℃/min to 600 ℃/min when the MgO content increases from 8% to 12%. Further increase of MgO to 16% slightly increases the critical cooling rate. Figure 5 shows the start crystallization temperature of the samples with varying Al_2O_3 and MgO contents. The start crystallization temperature under a lower cooling rate decreases approximately 100 ℃ when the Al_2O_3 content increases from 10% to 20%, while that increases approximately 120 ℃ when the MgO content increases from 8% to 16%. In addition, the start crystallization temperature decreases with the increase of cooling rate under each composition due to the nucleation and growth of crystals are closely related to the change of viscosity and undercooling degree of the samples, which is discussed in detail later. It should be noticed that the start crystallization temperature only slightly decreases with the increase of the cooling rate under higher MgO contents (e.g. 12% and 16%), which is still above 1200 ℃ at a condition close to the critical cooling rate. It means that cooling rate has a small effect on the crystallization temperature when the sample has a larger crystallization tendency.

Specifically, the increase of MgO content has a smaller effect on the start crystallization temperature than the change of Al_2O_3 content. This indicates that the crystallization ability greatly increases with the increase of MgO content, especially the MgO content is larger than 8%. Under different conditions of cooling rates and compositions, the final area fractions of crystallization phases can be obtained, as shown in Figure 6. The larger cooling rate, which result in lower crystallization ability and therefore smaller area fractions of crystallization phases can be obtained. This can partially reflect the nucleation and growth ability of crystals. The sample with more than 15% Al_2O_3 and less than 4% MgO under the CaO/SiO_2 ratio of 1 has the lowest crystallization tendency. The change of cooling rate and composition can result in the change of viscosity, melting temperature and structure, which can directly affect the crystallization behavior. The detailed discussion of different factors on the crystallization behaviour will be explained together with the TTT results in the following section.

3.2 Isothermal crystallization behavior

The TTT diagrams of the samples with varying Al_2O_3 and MgO contents are shown in Figure 7 and Figure 8. It can be seen that the crystallization period (time between the start crystallization and the end of crystallization) first decrease and then increase with the increase of temperature when the Al_2O_3 content is less than 10%. Higher temperature greatly delays the crystallization process due to the smaller supercooling degree and lower driving force for nucleation of crystals. This can be obviously seen in Figure 7 (c) and (d), since no crystallization can be observed after two hours

holding time when the temperature is larger than 1150 ℃ and 1100 ℃, respectively. With the increase of Al_2O_3 content, the crystallization process becomes much later as the start crystallization time becomes larger. Moreover, the crystallization period (time between the start of crystallization and the end of crystallization) expands with the increase of Al_2O_3 content. Specially, fully crystallization can not be observed when the Al_2O_3 content is 20%.

In terms of MgO effect, an opposite tendency can be obtained. When the MgO content is about 4%, crystallization can only be observed at lower temperatures, and the start crystallization time is much larger compared to those when the Al_2O_3 content is 20%. The start crystallization time becomes much smaller when the MgO content increases from 4% to 8%. With further increase of MgO content, the crystallization period getting shorter, indicating that the crystallization of inclusions occurred relatively easily. Moreover, the crystallization period of inclusions under different MgO contents is much shorter compared to those with different Al_2O_3 contents in the similar temperature range. This indicates that the change of MgO content has a larger effect on the crystallization rate compared to that of Al_2O_3. Thus, the increase of Al_2O_3 content and decrease of MgO content can greatly suppress the crystallization of the CaO-SiO_2- Al_2O_3-MgO system inclusions (CaO/SiO_2=1).

Besides, the TTT curve of inclusions shows multiple “C” shape, especially for the case of different MgO content, indicating that different crystallization processes occurred in different temperature zones. However, it is difficult to identify the different phases since single crystallization can not be easily obtained. Based on the TTT results, the proper holding temperature, time and inclusion composition can be controlled to obtain the optimized soaking process.

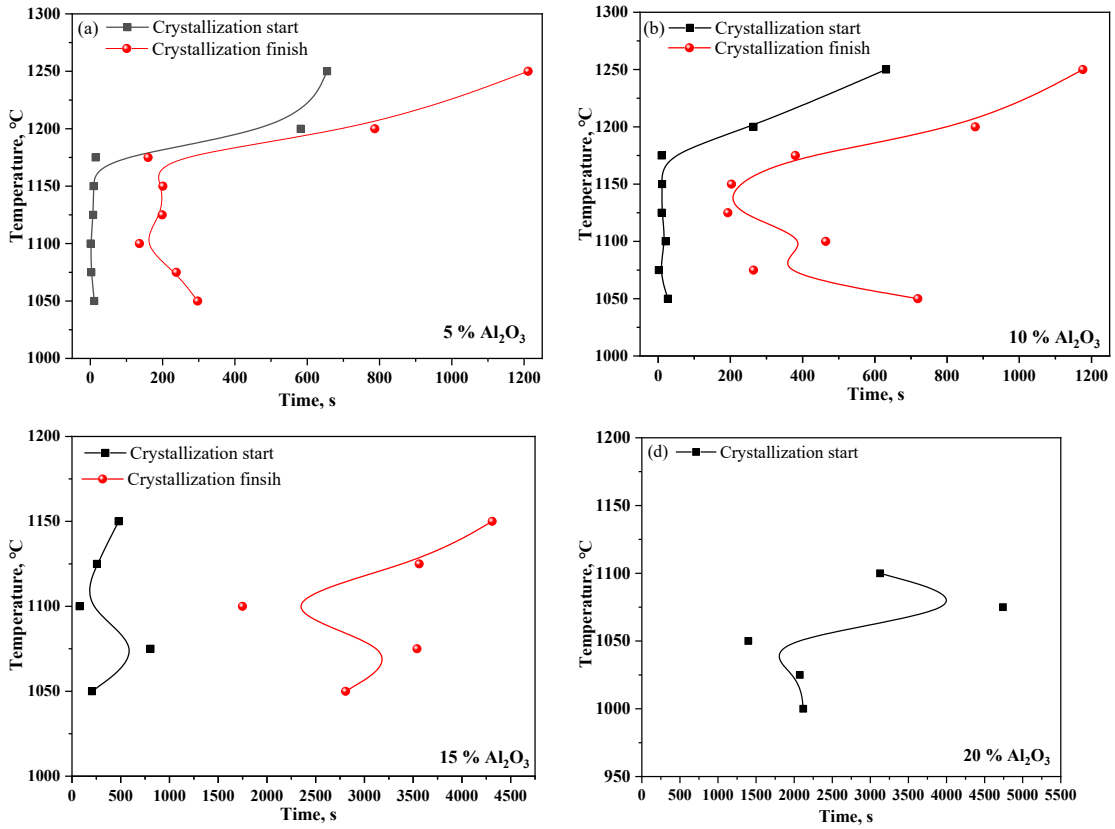

FIG 7 –TTT diagram for samples with varied Al_2O_3 contents (a) 5%, (b) 10%, (c) 15%, (d) 20%.

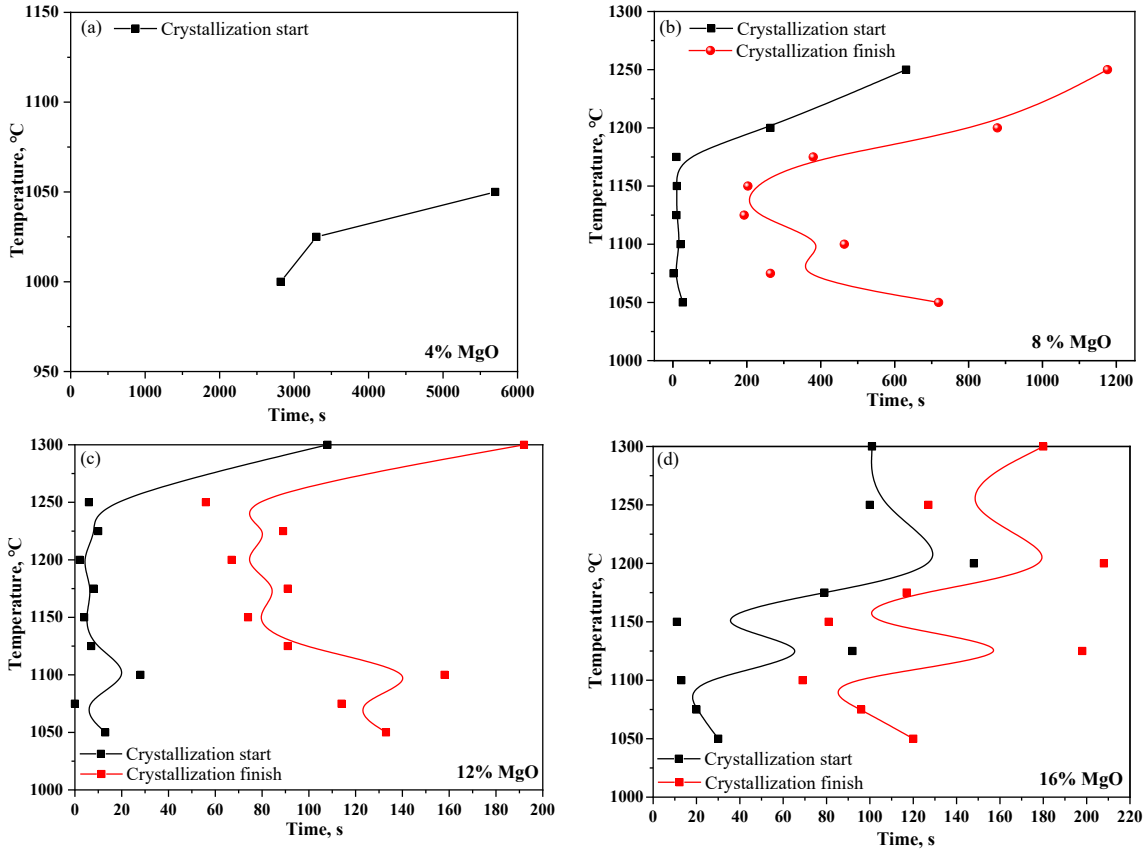

FIG 8 –TTT diagram for samples with varied Al_2O_3 contents (a) 5%, (b) 10%, (c) 15%, (d) 20%.

4. CONCLUSIONS

(1) The increase of MgO content increases the crystallization ability of CaO-SiO_2-Al_2O_3-MgO inclusions, while the increase of Al_2O_3 content has an opposite effect.

(2) The Al_2O_3 content of the system needs to be controlled larger than 15 wt.% and the MgO content should be kept at a small amount (less than 5 wt.%) to obtain low melting point plasticized CaO-SiO_2-Al_2O_3-MgO (CaO/SiO_2=1) system inclusions.

(3) The crystallization activation energy could semi-quantitatively characterize the crystal growth during the crystallization of inclusions, the viscosity can be used for predicting the crystallization tendency of inclusions.

ACKNOWLEDGEMENTS (USE 'HEADING 1' STYLE)

The authors are grateful for support from the National Natural Science Foundation of China (52304355 and U21A20113) and Japan Society for the Promotion of Science (JSPS).

REFERENCES

[1] L. Zhang and B.G. Thomas, State of the art in evaluation and control of steel cleanliness, *ISIJ international* **2003**, 43, 271-291.

[2] S. Y. Kitamura, Preface to the special issue on "fundamentals and applications of non-metallic inclusions in solid steel", *ISIJ international* **2011**, 51, 1943-1943.

[3] L. Zhang, C. Guo, W. Yang, Y. Ren, and H. Ling, Deformability of oxide inclusions in tire cord steels, *Metallurgical and Materials Transactions B* **2018**, 49, 803-811.

[4] Y. Yang, D. Zhan, G. Qiu, X. Li, Z. Jiang, and H. Zhang, Inclusion evolution in solid steel during rolling deformation: A review, *Journal of materials research and technology* **2022**, 18, 5103-5115.

[5] C. Chen, Z. Jiang, Y. Li, M. Sun, Q. Wang, K. Chen, and H. Li, State of the Art in the Control of Inclusions in Spring Steel for Automobile-a Review, *ISIJ International* **2020**, 60, 617-627.

[6] C. Chen, Z. Jiang, Y. Li, L. Zheng, X. Huang, G. Yang, M. Sun, K. Chen, H. Yang, and H. Hu, State of the art in the control of inclusions in tire cord steels and saw wire steels–A Review, *steel research international* **2019**, 90, 1800547.

[7] W.Y. Kim, K.S. Kim, and S.Y. Kim, Evolution of Non-metallic Inclusions in Si-Killed Stainless Steelmaking, *Metallurgical and Materials Transactions B* **2021**, 52, 652-664.

[8] S. Lyu, X. Ma, Z. Huang, Z. Yao, H.-G. Lee, Z. Jiang, G. Wang, J. Zou, and B. Zhao, Understanding the formation and evolution of oxide inclusions in Si-deoxidized spring steel, *Metallurgical and materials transactions B* **2019**, 50, 1862-1877.
[9] C. Bertrand, J. Molinero, S. Landa, R. Elvira, M. Wild, G. Barthold, P. Valentin, and H. Schifferl, Metallurgy of plastic inclusions to improve fatigue life of engineering steels, *Ironmaking & steelmaking* **2003**, 30, 165-169.
[10] Y. Meng, J. Li, K. Wang, and H. Zhu,Effect of the Bloom-Heating Process on the Inclusion Size of Si-Killed Spring Steel Wire Rod, *Metallurgical and Materials Transactions B* **2022**, 53, 2647-2656.
[11] P. Rocabois, J. Pontoire, J. Lehmann, and H. Gaye, Crystallization kinetics of Al_2O_3–CaO–SiO_2 based oxide inclusions, *Journal of non-crystalline solids* **2001**, 282, 98-109.
[12] Z. Li, W. Yang, H. Yao, and L. Zhang, Effect of Na2O addition on crystallization behavior and properties of 25 wt% Al_2O_3–SiO_2–CaO non-metallic inclusion-type oxides, *Ceramics International* **2022**, 48, 23849-23861.
[13] Y. Liang, C. Shi, Y. Huang, J. Ju, and J. Li, Effect of CaO/SiO_2 mass ratio and Li_2O on structure and phase precipitation behaviors of CaO–SiO_2–MgO–Al_2O_3 oxide inclusions, *Journal of Non-Crystalline Solids* **2022**, 597, 121911.
[14] C. Xuan, H. Shibata, S. Sukenaga, P.G. Jönsson, and K. Nakajima, Wettability of Al_2O_3, MgO and Ti_2O_3 by liquid iron and steel, *Isij International* **2015**, 55, 1882-1890.
[15] C. Xuan, H. Shibata, Z. Zhao, P.G. Jönsson, and K. Nakajima, Wettability of TiN by liquid iron and steel, *ISIJ International* **2015**, 55, 1642-1651.
[16] M. Tashiro, S. Sukenaga, and H. Shibata, Control of crystallization behaviour of supercooled liquid composed of lithium disilicate on platinum substrate, *Scientific reports* **2017**, 7, 6078.
[17] T.S. Kim and J.H. Park, Influence of Al_2O_3 and SiO_2 on the structure and viscosity of iron-compound bearing calcium-aluminosilicate slags, *Journal of Alloys and Compounds* **2022**, 916, 165328.
[18] J.F. Stebbins, J. Wu, and L.M. Thompson, Interactions between network cation coordination and non-bridging oxygen abundance in oxide glasses and melts: Insights from NMR spectroscopy, *Chemical Geology* **2013**, 346, 34-46.
[19] J.H. Park, D.J. Min, and H.S. Song, Amphoteric behavior of alumina in viscous flow and structure of CaO-SiO_2 (-MgO)-Al_2O_3 slags, *Metallurgical and Materials Transactions B* **2004**, 35, 269-275.
[20] Y. Sun, H. Wang, and Z. Zhang,Understanding the relationship between structure and thermophysical properties of CaO-SiO_2-MgO-Al_2O_3 molten slags, *Metallurgical and Materials Transactions B* **2018**, 49, 677-687.
[21] W. Yong-Quan, J. Guo-Chang, Y. Jing-Lin, H. Huai-Yu, and C. Hui, Raman scattering coefficients of symmetrical stretching modes of microstructural units in sodium silicate melts, *Acta Physica Sinica* **2005**, 54, 961.
[22] J.A. Baird, D. Santiago-Quinonez, C. Rinaldi, and L.S. Taylor, Role of viscosity in influencing the glass-forming ability of organic molecules from the undercooled melt state, *Pharmaceutical research* **2012**, 29, 271-284.